Numerical analysis of internal erosion impact on underground structures: Application to tunnel leakage

Jie Yang, Zhen-Yu Yin, Farid Laouafa, Pierre-Yves Hicher

Numerical analysis of internal erosion impact on underground structures: application to tunnel leakage

Jie YANG[1,2,3], Zhen-Yu YIN[1,*], Farid LAOUAFA[2], Pierre-Yves HICHER[3]

Affiliations:

[1] Department of Civil and Environmental Engineering, The Hong Kong Polytechnic University, Hung Hom, Kowloon, Hong Kong, China

[2] National Institute for Industrial Environment and Risks (INERIS), Verneuil-en-Halatte, France

[3] Research Institute of Civil Engineering and Mechanics (GeM), UMR CNRS 6183, Ecole Centrale de Nantes, France

[*] Corresponding authors: Dr. Zhen-Yu YIN, Tel: +852 3400 8470; Fax: +852 2334 6389; Email: zhenyu.yin@polyu.edu.hk; zhenyu.yin@gmail.com

Abstract: Water leakage is one of the most critical factors that affect the ground movement and structural behaviour during and after the construction of the shield tunnel. Currently, very limited attention has been paid to the effect of the loss of fine particles induced by the water leakage, namely the internal erosion. In this study, the evolution of soil porosity, gradation, seepage flow and the induced ground movement and lining stress change due to tunnel leakage has been numerically investigated using a novel coupled hydro-mechanical approach formulated within the continuous porous medium framework. The detachment and transport of fines particles within the seepage flow are considered by a four-constituent model of internal erosion. The induced influence on the soil mechanical behaviour is modelled by a critical-state-based constitutive model considering the evolution of the fines content. Using the proposed approach, the time-space evolution of the eroded zone and the hydro-mechanical response in the cases of a single tunnel and two crossing tunnels are identified. The results indicate that the commonly used pore pressure reduction-based method without considering internal erosion will under-estimate the leakage induced lining stress change and ground movement. Moreover, the influence of three-dimensional conditions, hydraulic boundary conditions and tunnel characteristics are highlighted.

Keywords: tunnel; silty sand; fine particles; finite element method; internal erosion; seepage

1 Introduction

With an increasing need for underground space, tunnels have been widely constructed in the past decades. During the service life of a tunnel, it has been observed that the post-construction ground movement due to tunnelling is significant and can continue for many years [1-3]. For example, after 16 years of operation of the shield tunnel in Shanghai China (from 1995 to 2011), the accumulated long-term settlement of the tunnel reached 290 mm [1]. The causes of tunnel settlement and soil deformation have been widely discussed, including the land subsidence, the variation of groundwater table, the water leakage, the dynamic response of train, etc. [4-7]. Water leakage into the tunnel is one of the most critical factors that affect the post-construction ground movement [8, 9] and lead to an increase in the additional inner forces of the tunnel lining [10].

An early effort to consider the effect of leakage on the tunnel and the surrounding soil was to estimate the leakage-induced pore pressure reduction based on Darcy's law [11-14]. The water leakage through the linings was usually modelled by increasing uniformly the equivalent permeability of the lining along the tunnel circumference under a given water inflow rate [15-18]. However, the leakage in a shield precast tunnel in saturated soil is often found at localized openings such as the segmental joints, cracks, and grouting holes. Recently, by applying the pore pressure reduction method using finite element analysis, Zhang et al. [19] studied the impact of partial leakage on a shield precast tunnel in saturated soil. The results demonstrated that the uniform tunnel leakage assumption in isotropic soils would overestimate the induced tunnel and ground settlement.

However, in terms of leakage-induced surrounding soil degradation, very limited attention has been paid to the effect of the loss of fine particles induced by the water leakage. The leakage of groundwater through the cracks and joints of lining commonly carries fines in the form of silt and clay from the surrounding ground, leading to the internal erosion of the surrounding soil [20]. The increase of void ratio and the change of soil gradation due to the loss of fines affect the mechanical behaviour of the surrounding soil [21-24]. Meanwhile, the change of porosity influences the permeability of the soil and, therefore, the erosion process. However, up to now, the hazards induced by internal erosion have been mainly studied for earth dams [25-29]. More attention should be paid to tunnel engineering. Zhang et al. [30] investigated the mechanism of seepage erosion around shield tunnels using the CFD-DEM method via PFC3D at the scale of a representative elementary volume. However, even though the discrete methods

can describe more accurately the physical mechanisms occurring within granular materials, they are yet restricted to problems with a too-small number of particles. They do not provide, therefore, a sufficiently accurate representation of the physical problems at the spatial scale of a geotechnical structure. Consequently, at the scale of a geotechnical structure, there is a critical need to develop alternative methods to take the internal erosion into consideration for accurately determining the leakage-induced impacts on the underground structures.

In this study, based on porous continuous medium theory, the effect of leakage on tunnels constructed in silty sand has been numerically investigated by a coupled hydro-mechanical approach, considering both the internal erosion phenomenon induced by the local inflows of groundwater and the mechanical consequences of erosion on the surrounding soil.

The development of the coupled hydro-mechanical model considering internal erosion and its mechanical consequence is first presented. The proposed model consists of a single unified system of equations derived from the mass balance based on the mixture theory, which allows considering convective dominant transport of fluidized fines within the fluid flow, the transition of the fine particles from solid to fluidized particles phase and the effect of deformation on porous flow. The mechanical degradation induced by the loss of fine particles is considered by adopting a sand-silt mixture model proposed by Yin et al. [21, 22]. The model has been implemented into a finite element code, and then improved by using the stabilized finite element technique to eliminate the spurious numerical oscillations in solving the convection dominant flow of transported particles. The second part focuses on the applications of the hydro-mechanical model in simulating the ground and tunnel responses induced by tunnel leakage in the 2D and 3D conditions. The erosion and pore pressure reduction induced responses are analyzed. The influence of the 3D condition and the boundary conditions are emphasized.

2 Coupled hydro-mechanical model for internal erosion and mechanical consequence

The theory of mixtures provided a macroscopic description of the composition, the relative motion and the interaction in soils. It has been shown that the balance of mass of any phase or constituent can be expressed in terms of referential coordinates of any other phase or constituent [31]. In the present study, the mass balance equations based on the mixture theory are adopted to describe the motion of a liquid phase relative to a solid phase in a non-rigid soil.

Moreover, the rate of erosion defined by the erosion law is considered through the source term in the mass balance equations.

2.1 Mass balances and transported particles

The saturated porous medium can be considered as a material system composed of 4 constituents in solid and liquid phases: the stable fabric of the solid skeleton (*ss*), the erodible fines (*se*), the fluidized fines (*fp*) and the pure fluid (*ff*). The fines can behave either as fluid-like (described as fluidized fines) or as solid-like (described as erodible fines) material. The description of transport phenomena occurring in this system can be obtained from mass balance equations based on the mixture theory [32-35]. Starting from the macroscopic balance of the mixture system, in a representative elementary volume (REV), the mass balances for the mixture system can be expressed as:

$$\frac{\partial\left(n^i\right)}{\partial t}+\operatorname{div}\left(n^i\mathbf{v}^i\right)=n^{ex,i} \quad \text{.....(1)}$$

where n^i and $\mathbf{v}^i$ denote, respectively, the volume fraction and the velocity of the constituent $i=\{ss,se,fp,ff\}$, $n^{ex,i}$ is the term of the volume of mass exchange among the constituents. The transition of the fine particles from solid to fluidized particles leads to:

$$-n^{ex,fp}=n^{ex,se}=\hat{n},\ n^{ex,ss}=0,\ n^{ex,ff}=0 \quad \text{.....(2)}$$

Therefore, the transport of fluidized fines in soil mass including the transformation between fluid-like fines and solid-like fines can be represented by a set of partial differential equations (PDE), the balance of volume of the solid phase (solid skeleton and erodible fines), the erodible fines, the fluidized particles and the mixture system can be expressed respectively as:

$$-\frac{\partial\phi}{\partial t}+\operatorname{div}\left(\mathbf{v}_s\right)-\operatorname{div}\left(\phi\mathbf{v}_s\right)=\hat{n} \quad \text{.....(3)}$$

$$\frac{\partial\left(f_c\right)}{\partial t}-\frac{\partial\left(f_c\phi\right)}{\partial t}+\operatorname{div}\left(f_c\mathbf{v}_s\right)-\operatorname{div}\left(f_c\phi\mathbf{v}_s\right)=\hat{n} \quad \text{.....(4)}$$

$$\frac{\partial\left(c\phi\right)}{\partial t}+\operatorname{div}\left(c\mathbf{q}_w\right)+\frac{\partial\left(c\phi\mathbf{v}_s\right)}{\partial t}=-\hat{n} \quad \text{.....(5)}$$

$$\operatorname{div}\left(\mathbf{q}_w\right)+\operatorname{div}\left(\mathbf{v}_s\right)=0 \quad \text{.....(6)}$$

where $f_c\left(x,t\right)$, $\phi\left(x,t\right)$ and $c\left(x,t\right)$ are the fraction of erodible fines, the porosity and the concentration of the fluidized fines at any point in time; $\hat{n}$ is the source term describing the

rate of transformation between fluid-like fines and solid-like fines; $\mathbf{v}_s$ is the velocity of the soil skeleton; $\mathbf{q}_w(x,t)$ is the total discharge of the pore fluid assumed to be governed by Darcy's law :

$$\mathbf{q}_\mathbf{w} = -\frac{k}{\eta_k \bar{\rho}}\left(\mathbf{grad}(p_w) - \bar{\rho}\mathbf{g}\right) \quad (7)$$

where k is the intrinsic permeability of the medium; η_k is the kinematic viscosity of the fluid; p_w is the pore fluid pressure; $\mathbf{g}$ is the vector of the gravity field; $\bar{\rho}(c)$ is the density of the mixture defined as:

$$k = k_0 \frac{\phi^3}{(1-\phi)^2} \quad (8)$$

$$\bar{\rho} = c\rho_s + (1-c)\rho_f \quad (9)$$

with ρ_s and ρ_f denote the density of the solid and the fluid; k_0 denote the initial permeability according to the Kozeny-Carman relationship [36].

2.2 Rate of erosion

To close the set of PDE of Eqs. (3)-(5), the variable $\hat{n}$ which determines the rate of transformation between fluid-like and solid-like fines should be defined by an appropriate erosion model. According to experimental observations, the internal erosion of soil is mainly driven by the discharge of the pore fluid and the amount of erodible fine particles. Therefore, for the sake of simplicity, a linear erosion law [37] has been adopted as follows:

$$\hat{n} = -\lambda_e f_c |\mathbf{q}_\mathbf{w}| \quad (10)$$

where λ_e is an erosion constant. Over the years, different expressions for the erosion model have been proposed [20, 34, 35, 37-40], for example, Cividini et al. [41] has proposed that the ultimate fine content fraction after a long seepage period can be decreased with the increase of the hydraulic gradient as:

$$f_{c\infty} = f_{c0}\left[(1-\alpha_1)\exp\left(-|\mathbf{q}_\mathbf{w}| \times 10^{\alpha_2}\right) + \alpha_1\right] \quad (11)$$

where f_{c0} is the initial fine content fraction, α_1 and α_2 are material constants. The term $f_{c\infty}$ corresponds to the residual fine content fraction. It can be seen that for a fixed initial fine content fraction and fixed hydraulic gradient, the ultimate fine content fraction, as well as the residual fines content, are constant. Therefore, in the following analyses, a fixed residual fines content has been introduced artificially. Moreover, the present study does not focus on comparing different erosion models since the numerical approach suggested here is modular. It is possible to choose the most appropriate erosion model for various applications. The erosion model can be improved and calibrated by experimental data in future case studies.

2.3 Critical state-based soil model considering the change of fines content

The linear momentum balance of the mixture system under isothermal and quasi-static conditions is adopted to describe the hydro-mechanical coupling for a saturated deformable porous medium [42]:

$$\operatorname{div}\left(\boldsymbol{\sigma}_i\right)+\mathbf{w}_i+\hat{\mathbf{p}}_i=\rho_i\mathbf{a}_i,\ \sum_i\hat{\mathbf{p}}_i=0 \quad \text{.....(12)}$$

where $\boldsymbol{\sigma}_i$, $\mathbf{w}_i$, ρ_i and $\mathbf{a}_i$ are respectively the partial Cauchy stress tensor, unit weight, density and acceleration of solid or liquid phase; $\hat{\mathbf{p}}_i$ is the interaction momentum production between solid and liquid phases. The partial Cauchy stresses $\boldsymbol{\sigma}_i$ for the two phases are derived as follows for a fluid-saturated medium [33]:

$$\boldsymbol{\sigma}_s=\boldsymbol{\sigma}'-\left(1-\phi\right)p_w\mathbf{I},\ \boldsymbol{\sigma}_l=-\phi p_w\mathbf{I} \quad \text{.....(13)}$$

with $\boldsymbol{\sigma}'$ denotes the effective stress tensor responsible for solid skeleton's deformation that needs to be described by an appropriate constitutive model. Thereafter, the set of equations (6) -(5) can be closed by:

$$\operatorname{div}\left(\boldsymbol{\sigma}'-p_w\mathbf{I}\right)+\mathbf{w}=0 \quad \text{.....(14)}$$

A non-associated critical state-based elastoplastic model, namely the basic SIMSAND model [43-45], has been extended for the sand-silt mixture to evaluate the mechanical response of the solid phase to the loss of fines content induced by internal erosion [22] (summarized in Appendix).

In order to unify the mechanical behaviour of a sand-silt mixture from silt to sand or sand to silt, the critical state line in the *e-p'* plane has been assumed to be related to the amount of the solid-like fines content (see Eqs. (15) and (16)). Consequently, the improved sand-silt mixture

model is able to consider the effect of the loss of fines content on the mechanical behaviour of the soil induced by internal erosion.

The adopted non-linear critical state line in the e-p' plane can be expressed as [46] :

$$e_c = e_{cr0} - \lambda \left(\frac{p'}{p_{at}} \right)^{\xi} \quad \text{..... (15)}$$

where the reference critical void ratio e_{cr0} determines the position of the CSL in the *e-p'* plane, it denotes the void ratio where the mean effective stress p'=0. p_{at} denotes the atmospheric pressure. λ and ξ denotes material parameters.

Experimental studies demonstrated that the mechanical behaviour of sand-silt mixtures is closely related to the proportions of sand and silt. Yin et al. [21, 22] proposed a formulation that links the inter-grain contact index with the reference critical void ratio e_{cr0} to determine the position of the CSL of sand-silt mixtures for different fines contents:

$$e_{cr0} = \left[e_{hc,cr0} \left(1 - f_c\right) + a f_c \right] \frac{1 - \tanh\left[\zeta \left(f_c - f_{th} \right)\right]}{2} + e_{hf,cr0} \left(f_c + \frac{1 - f_c}{\left(R_d\right)^m} \right) \frac{1 + \tanh\left[\zeta \left(f_c - f_{th} \right)\right]}{2} \quad \text{..... (16)}$$

The formulation was structured by linking the coarse grain skeleton (i.e., silty sand) and the fine grain skeleton (i.e., sandy silt) using the hyperbolic tangent function $\tanh x = \left(e^{2x} - 1\right) / \left(e^{2x} + 1\right)$. $e_{hf,cr0}$ and $e_{hc,cr0}$ denotes the reference critical void ratios for pure silt and pure sand, respectively. a, ζ, R_d, m and f_{th} are material parameters.

In this study, the water pressure at the leakage points was assumed to be zero. In terms of the hydro-mechanical coupling effect of the proposed modelling approach, it can be conceptually divided into two parts: first, the loss of fines contents induced by the internal erosion will lead to an evolution of the porosity, as well as the permeability (according to Eq. (11)) and, consequently, to the change of pore pressure gradient or seepage velocity; in parallel, the evolution of fines content affects (a) the void ratio and (b) the location of the critical state line, obtained by combining Eq. (15) and (16) for a soil mixture, leading to the mechanical degradation of the eroded soil.

3 Numerical integration

3.1 Standard Galerkin-weighted residual method

By combining the balance and constitutive equations, the governing equations for the Initial Boundary Value Problem (IBVP) of internal erosion can be formulated as follows:

$$\left(\sigma'_{ij} - p_w\right)_{,j} + w_j = 0 \quad \text{..... (17)}$$

$$\operatorname{div}\left(v_s\right) + \operatorname{div}\left(q_w\right) = 0 \quad \text{..... (18)}$$

$$-\frac{\partial(\phi)}{\partial t} + \operatorname{div}\left(v_s\right) - \operatorname{div}\left(\phi v_s\right) + \lambda_e f_c \left|q_w\right| = 0 \quad \text{..... (19)}$$

$$\frac{\partial(c\phi)}{\partial t} + \operatorname{div}\left(cq_w\right) + \operatorname{div}\left(c\phi v_s\right) - \lambda_e f_c \left|q_w\right| = 0 \quad \text{..... (20)}$$

$$q_w + \frac{k}{\eta_k \bar{\rho}}\left(\operatorname{grad}\left(p_w\right) - \bar{\rho}\mathbf{g}\right) = 0 \quad \text{..... (21)}$$

where σ'_{ij} denotes the effective stress of soil, w_j denotes the self-weight. The primary unknowns are $\mathbf{u}(\mathbf{x},t)$, $p_w(\mathbf{x},t)$, $\phi(\mathbf{x},t)$, $c(\mathbf{x},t)$ and $q_w(\mathbf{x},t)$, which denote respectively the soil skeleton displacement, the pore pressure, the porosity, the concentration of fluidized fines particles and the flow rate. For the sake of readability, the time t and space $\mathbf{x}$ variables have been omitted in the equations.

The governing PDEs of the non-linear transient problem can be solved using the standard Galerkin-weighted residual method via ABAQUS-UEL [47] by defining a new type of element according to the user-defined governing equations and degrees of freedom (DOFs). The user-defined governing PDEs are then solved by the solver of ABAQUS by using Newton's method. New types of isoparametric elements have been developed and implemented into ABAQUS via the UEL subroutine, with 7 DOFs $\left(\mathrm{u}_x, \mathrm{u}_y, p_w, \phi, c, \mathrm{q}_{wx}, \mathrm{q}_{wy}\right)$ for the plane strain and flow condition and 9 DOFs for the three-dimensional condition $\left(\mathrm{u}_x, \mathrm{u}_y, \mathrm{u}_z, p_w, \phi, c, \mathrm{q}_{wx}, \mathrm{q}_{wy}, \mathrm{q}_{wz}\right)$.

3.2 Stabilized finite element method

When using the standard Galerkin-weighted residual method for solving convection dominated flows (Eq. (20)), numerical oscillations has been noticed, which affects the computational accuracy and efficiency [48, 49]. The increase of the Péclet number will make the oscillations became more significant [50-52], leading to the corruption of solutions. The Péclet number can be reduced by refining the mesh to eliminate such numerical oscillations [48], but leading to

prohibitive computational cost at the scale of real soil structure. An alternative method regardless of mesh refinement is therefore needed.

Yu and Heinrich [53, 54] proposed a Petrov-Galerkin weighted residual method for solving the convection dominated flows. Perturbed weighting functions are introduced in the weighted residuals formulation as an added local anisotropic balancing diffusion and an added dispersion in the direction of the convective motion to eliminate the artificial diffusion of the solution and avoid the numerical dispersion.

By applying the Petrov-Galerkin weighted residual method, the weak form of Eq.(20) becomes:

$$\begin{aligned}
&\frac{1}{\Delta t}\int \phi\left(\mathbf{N}^N+\alpha\frac{h}{2}\frac{\mathbf{v}}{|\mathbf{v}|}\frac{\partial \mathbf{N}^N}{\partial \mathbf{x}}\right)\mathbf{N}^M dV\left(c^{M,t+\Delta t}-c^{M,t}\right)\\
&+\frac{1}{2}\int\left(\mathbf{N}^N+\alpha\frac{h}{2}\frac{\mathbf{v}}{|\mathbf{v}|}\frac{\partial \mathbf{N}^N}{\partial \mathbf{x}}\right)\mathbf{v}\frac{\partial \mathbf{N}^M}{\partial \mathbf{x}}dV\left(c^{M,t+\Delta t}+c^{M,t}\right)\\
&-\frac{\beta h}{4}\int\frac{\mathbf{v}}{|\mathbf{v}|}\frac{\partial \mathbf{N}^N}{\partial \mathbf{x}}\mathbf{v}\frac{\partial \mathbf{N}^M}{\partial \mathbf{x}}dV\left(c^{M,t+\Delta t}-c^{M,t}\right)\\
&+\int\left(\mathbf{N}^N+\alpha\frac{h}{2}\frac{\mathbf{v}}{|\mathbf{v}|}\frac{\partial \mathbf{N}^N}{\partial \mathbf{x}}\right)\left(\hat{n}+c\frac{\Delta\phi}{\Delta t}\right)dV=0
\end{aligned} \quad \text{..... (22)}$$

where $\mathbf{N}^N$ denotes the shape function, $\mathbf{v}$ denotes the average fluid velocity at the element centroid; $|\square|$ is the Euclidean norm; h is the characteristic element length, defined as:

$$h=\sum_{\alpha}|h_a| \text{ and } h_a=\mathbf{h}_\alpha\cdot\frac{\mathbf{v}}{|\mathbf{v}|} \quad \text{..... (23)}$$

with $\mathbf{h}_\alpha$ denotes the isoparametric passing through the element centroid, h_α denotes the projection of $\mathbf{h}_\alpha$ in the direction of the fluid flow at the element centroid.

According to Yu and Heinrich [53, 54], the perturbation constants α and β can be given as:

$$\alpha=\coth\frac{\gamma}{2}-\frac{2}{\gamma} \text{ and } \beta=\frac{C}{3}-\frac{2}{\gamma}\frac{\alpha}{C} \quad \text{..... (24)}$$

$$\gamma=|\mathbf{v}|h\frac{\rho c}{k} \text{ and } C=|\mathbf{v}|\frac{\Delta t}{h} \quad \text{..... (25)}$$

with γ denotes the local Péclet number and C denotes the local Courant number of the element.

4 Numerical analysis of leakage in a single tunnel

4.1 Description of the problem

This is a simple but most general case in urban tunnels. According to Zhang et al. [19], the depth of shield tunnels in Shanghai varies from 9 to 15 m. In this study, the tunnelling process and the induced ground movement and the tunnel squat were not considered. The ground and tunnel responses analyzed here are therefore the increments induced by the tunnel leakage. Based on a typical shield tunnel in Shanghai [19], a sketch of the investigated tunnel is illustrated in Figure 1, the depth of the tunnel center is 13.6 m, the inner diameter of the tunnel is 5.5 m, and the thickness of the tunnel lining is 0.35 m.

According to Dammyr et al. [55], the typical leakage points in the entire tunnel linings are located at grouting sockets, cracks in the concrete segments and segmental joints as presented in Figure 2. In practice, most of the leakage was observed at segmental joints [56]. Zhang et al. [19] inspected the leakage of groundwater into a metro line of shield tunnel built in Shanghai. They reported that more than 89% of the water inflow was observed at the segment joints in the inspected shield tunnel.

The numerical approach presented above was applied to study the hydro-mechanical response of a shield tunnel installed within a saturated silty sand layer and experiencing a local internal erosion induced by the leakage of groundwater. It should be noted that the proposed approach has been verified in previous studies at the REV scale [22, 24, 35], however, due to the lack of well-documented test data and in-situ data for the case of tunnel leakage, the analysis in this section is a theoretical study. The influence of grouted area, in-situ soil stratum and properties, and the geometric dimension of leakage point are not considered. All results are compared with the commonly used pore pressure reduction-based method. It aims to theoretically identify the role of internal erosion in tunnel leakage and to provide a novel numerical approach to estimate more accurately the impact of water leakage on the shield tunnel and its surroundings.

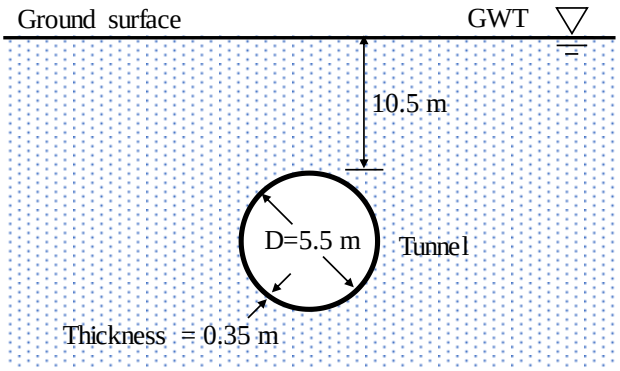

Figure 1 Scheme of the shield tunnel in the numerical analysis

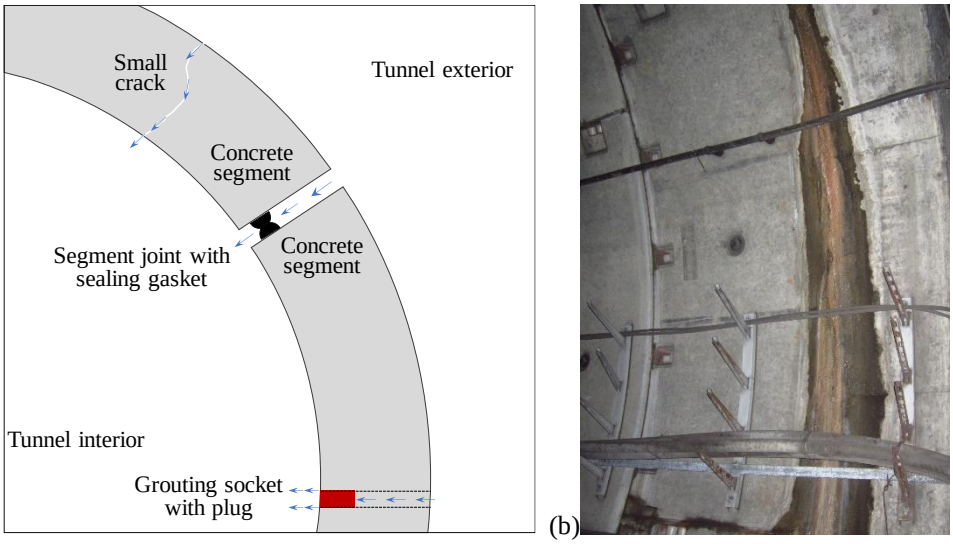

Figure 2 Illustration of leakage points in the shield precast tunnel: (a) re-annotated after Dammyr et al. [55]; (b) Leakage of the shield tunnel in saturated soils in Shanghai

4.1.1 Geometry of the numerical model

According to Yang et al. [25, 29], the three-dimensional (3D) condition is a significant factor that affects the process of internal erosion. The analysis was therefore carried out in the 2D and 3D conditions. The features of the studied model are shown in Figure 3. The depth of the top of the tunnel was 10.5m. The external and internal diameters of the circular cross-section of the shield tunnel were 6.2m and 5.5m, respectively. The thickness of the concrete segment was 0.35 m. According to the symmetric condition, for the 2D model, only half of the specific domain was modelled with 3456 hydro-mechanical coupled elements; for the 3D model, only one-quarter of the specific domain was modelled with 72576 coupled elements, shown in Figure 3. The tunnel lining was assumed to be linear elastic. The boundary conditions were taken as rollers on the left and right boundary of the model and fully fixed at the base of the model.

4.1.2 Hydraulic boundary condition

The groundwater level was supposed to be located at the ground surface. In this theoretical analysis, the leakage points were assumed to be located at the top of the tunnel, as shown in Figure 4, the influence of the location of leakage point can be studied in the future. In this case, the leakage point is an open boundary where the pore pressure is assumed to be equal to the atmospheric pressure, the groundwater can flow out freely, the corresponding initial steady flow rate is 0.024 $m^3/m^2/d$. In practice, the flow rate at the leakage point can also be given as the hydraulic boundary condition instead of assigning the boundary water pressure. It should be noted that, under plane strain and flow conditions, the leakage was assumed to act along a segment of lining in the longitudinal direction of the tunnel.

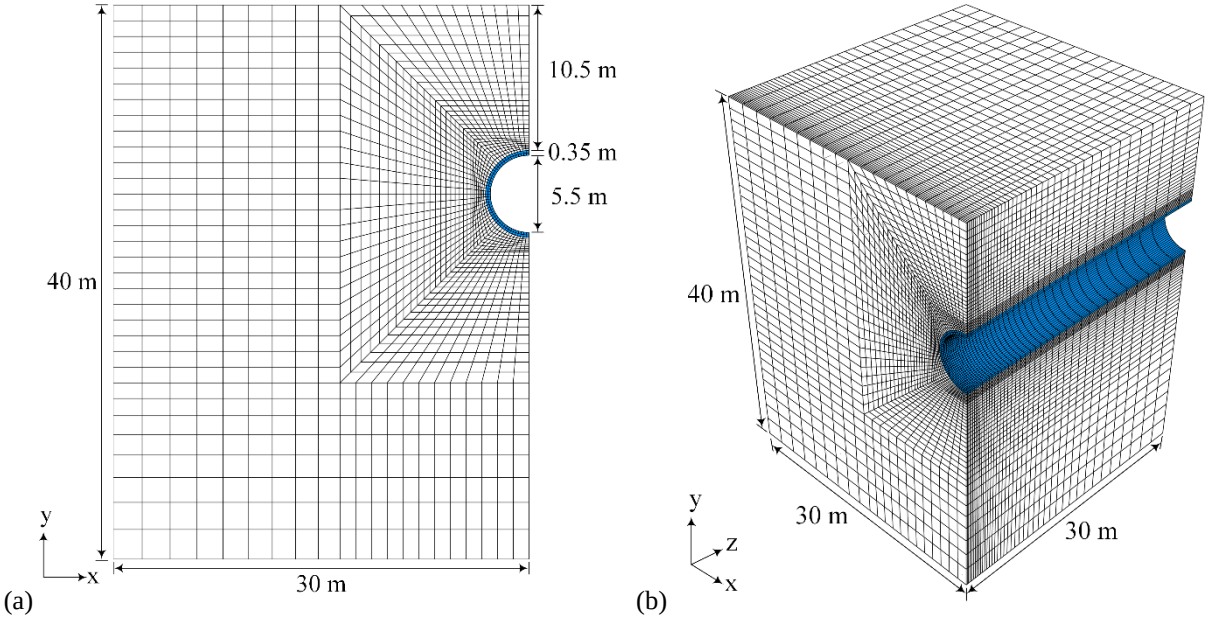

Figure 3 Mesh of the numerical models: (a) 2D model (1/2 model due to symmetry); (b) 3D model (1/4 model due to symmetry)

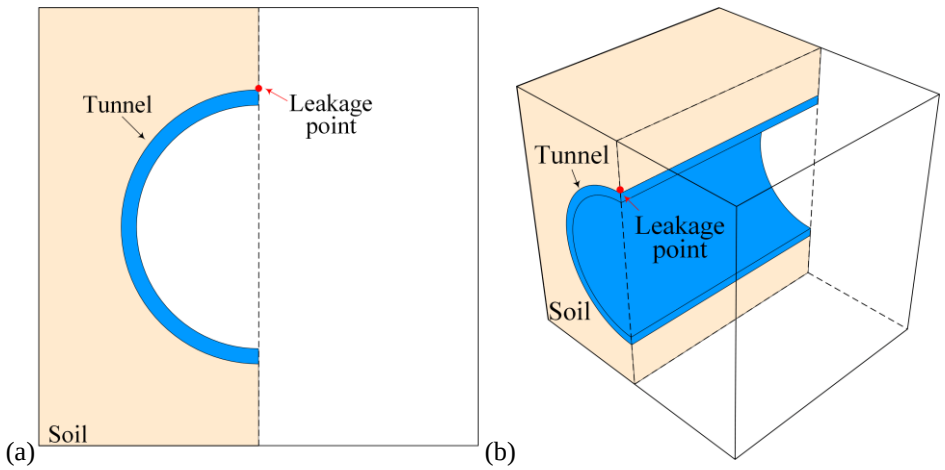

Figure 4 leakage location at tunnel lining: (a) 2D model; (b) 3D model

4.1.3 Initial stress state

Note that the focus of this study is to identify the role of fine loss in tunnel leakage induced ground deformation and tunnel bending moment change, where the leakage process is mainly controlled by the erosion law and hydraulic gradient. Moreover, the impact of the stress state especially the confining pressure on the erodibility of fine particles still remains unclear as the results in the literature [57-60] present contradictions. Therefore, a stress-state-independent erosion law was adopted in the present study and the excavation history of the tunnel and the installation process of the linings were omitted. The excessive pore pressure induced by the excavation process was assumed to be entirely dissipated before the leakage analysis. The groundwater table was at the ground surface. The effective stresses were initialized within the soil under gravity with the coefficient of earth pressure K_0 assumed to be 0.5. The deformation was reset to zero after the stress initiation. The interaction between the lining and the soil was defined by the contact properties in the normal and tangential directions of the contact surface. In the normal direction, the contact was assumed to be rigid, neither penetration nor separation was allowed. In the tangential direction, the contact was assumed to be rough, preventing any relative sliding motion between two contacting surfaces to take place.

4.1.4 Model parameters

The fines-dependent critical-state-based model was adopted for the elements of the soil. In this study, the physical properties and the material parameters corresponding to the Ottawa 50/200 sand - silt mixture [22] are adopted, as summarized in Table 1 and Table 2, with initial void ratio $e_0 = 0.5$, initial fines content $f_{c0} = 0.33$ and initial conductivity 1.0×10^{-8} m/s . Due to the lack of experimental data of real tunnel leakage case, the erosion constant λ_e was determined in an empirical manner, and the residual fines content $f_{c,r}$ [61] was fixed to 0.13. Note that an efficient optimization-based procedure for identifying the parameters of a hydro-mechanical model for internal erosion has been proposed recently by Yang et al. [62]. It can be used for a possible calibration of a tunnel leakage case in the future with well-documented laboratory and in-situ erosion test data.

The segments of tunnel lining made of precast reinforced concrete were assumed to be linear elastic. The reduction of tunnel stiffness induced by the joints of the segments was considered by reducing the stiffness of the continuous solid elements for tunnel lining [63-65]. Accordingly, Young's modulus of the linear elastic continuous solid elements of tunnel lining was set to 18 GPa with the Poisson’s ratio equal to 0.2.

Table 1 Material constants of soil and fluid

Density of fluid	ρf	1.0 g/cm^3
Density of solids	ρ_s	2.65 g/cm^3
Kinematic viscosity of the fluid	η_k	5.0E-6 m^{2}s^{-1}

Table 2 Model parameters of Ottawa sand

Elastic parameters			Plastic parameters			CSL-related parameters				Fines parameters					Erosion parameter
K_0/MPa	ν	n	k_p	A_d	ϕ_u	$e_{hc,cr0}$	$e_{fc,cr0}$	ξ	λ	a	m	f_{th}	R_d	ζ	λ_e
130	0.25	0.52	0.0017	1	32	0.805	1.03	0.196	0.081	0	0.7	0.3	4	20	0.05

4.2 Hydro-mechanical responses

Figure 5 and Figure 6 show the time variation of the fines content and the corresponding displacement magnitude fields during the leakage process in the 2D and 3D conditions, respectively. It was observed that induced by the internal erosion, the fines content that was initially uniform throughout the whole domain, began to decrease with time. The decrease was critical in the vicinity of the cavity, which created a highly eroded zone. At places where the fines content reached its residual value, it was assumed that the erosion process was balanced by the filtration process and, consequently, the void ratio would no longer change, but the size of the eroded area would continue to develop. Compared with the results in the 2D condition, the eroded zone in 3D was more localized around the leakage point and developed more slowly. An area with a significant ground settlement was found above the leakage point, indicating the inception of a sinkhole as the result of internal erosion.

It should be noticed that the calculated settlement induced by the tunnel leakage appears to be small (2.2 cm) compared to the observed long-term settlement of the shield tunnel in Shanghai (29 cm after 16 years of operation [1]). According to Shen et al. [1], the main mechanisms of settlement include the land subsidence, the disturbance from tunneling and nearby construction, the groundwater infiltration and change in hydraulic regime, and the cyclic load of train. It is thus reasonable that the calculated settlement is smaller than the actual observation in Shanghai. The aim of this study was mainly to provide a novel method to identify the potential consequences of internal erosion induced by tunnel leakage. A possible calibration of tunnel leakage in Shanghai can be performed in the future with well-documented laboratory and in-situ erosion test data.

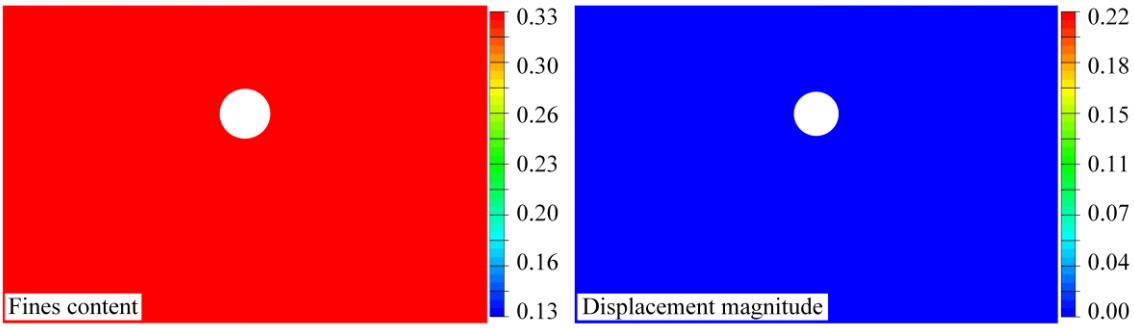

(a) Time = 0.0 years

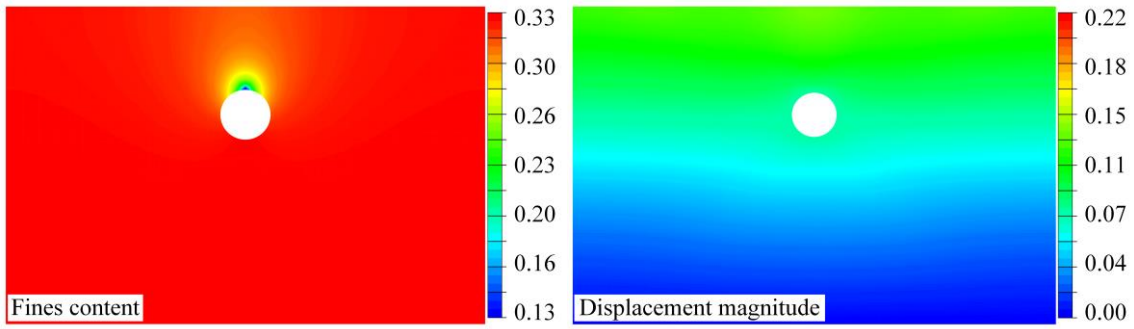

(b) Time = 7 years

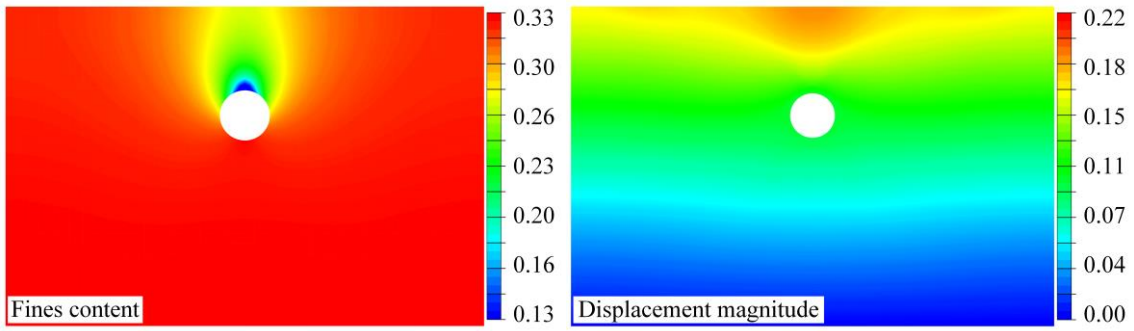

(c) Time = 14 years

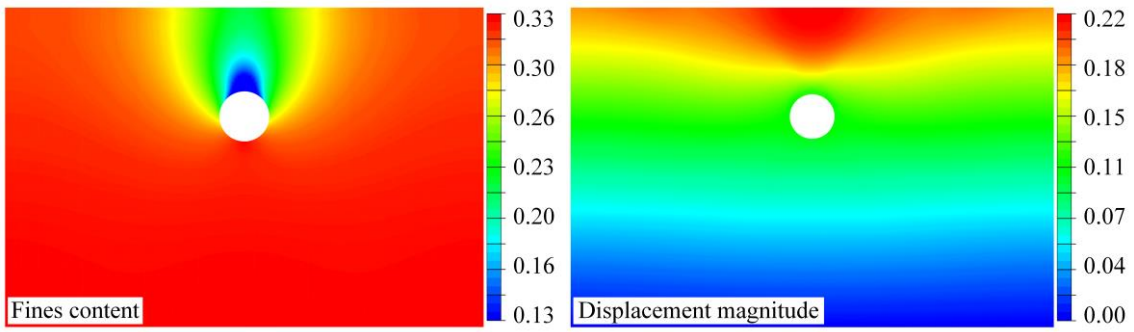

(d) Time = 20 years

Figure 5 Spatial distribution of fines content f_c and the corresponding displacement magnitude (unit: 10^{-1}m) in 2D condition at different times during the leakage

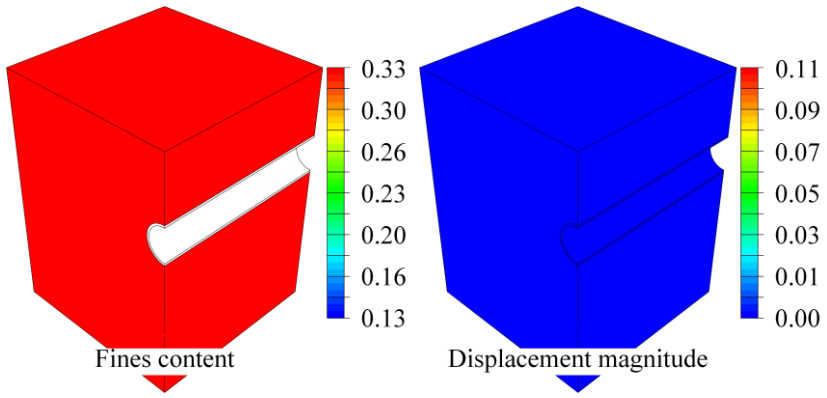

(a) Time = 0.0 years

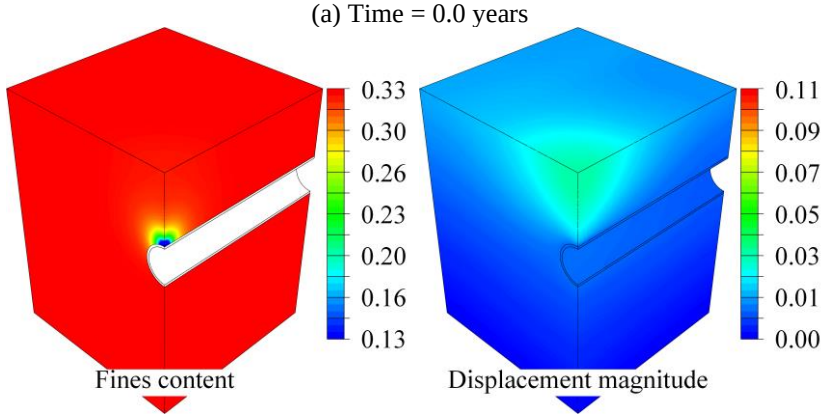

(b) Time = 7 years

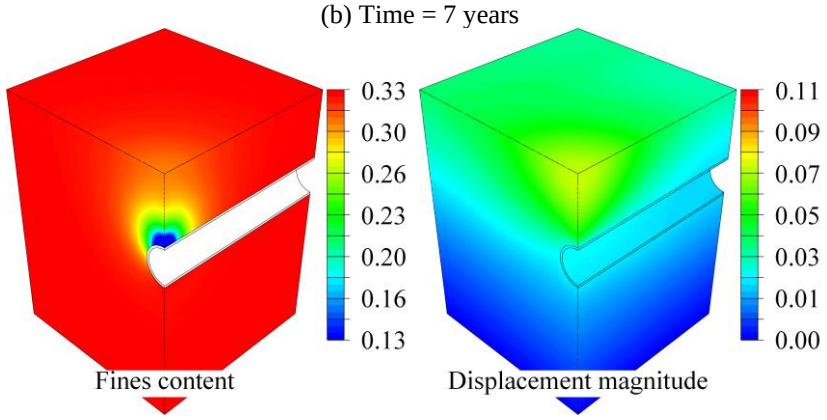

(c) Time = 14 years

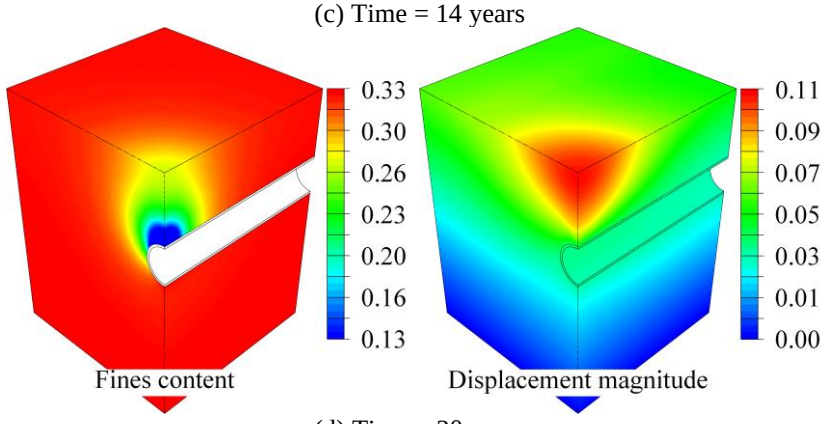

(d) Time = 20 years

Figure 6 Spatial distribution of fines content f_c and the corresponding displacement magnitude (unit: 10^{-1}m) in 3D condition at different times during the leakage

Figure 7 shows the profiles of pore pressure distribution above the tunnel for the calculations in 2D conditions. It was observed that due to the water leakage, the pore pressure, which was

initially linear with depth, was decreased around the leakage point. The internal erosion induced by the leakage of the tunnel would increase the voids as well as the permeability of the eroded soil, leading to the continuous redistribution of pore water pressure. However, for the case where the erosion was not considered, the fluid flow reached steady-state quickly and the pore pressure remained constant thereafter.

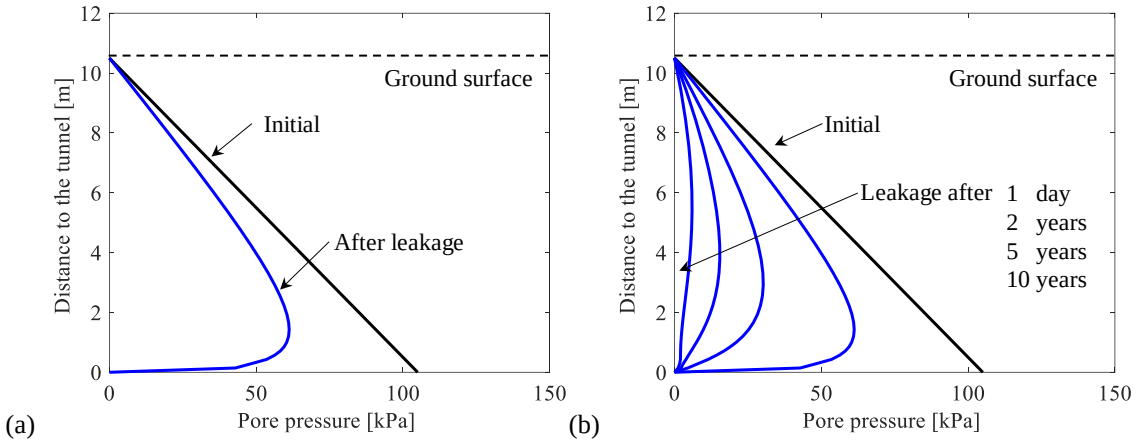

Figure 7 Profiles of pore pressure distribution above the tunnel: (a) without erosion; (b) with erosion

Figure 8 shows the movement of CSL at the monitored point A located at 1.2m above the top of the tunnel in plane strain and flow conditions Due to the loss of fine particles, the void ratio, as well as the location of CSL in the e - p' plane kept changing. It was observed that for the monitored point, the density state changed from slightly dense to loose state, which would lead to the degradation of soil strength.

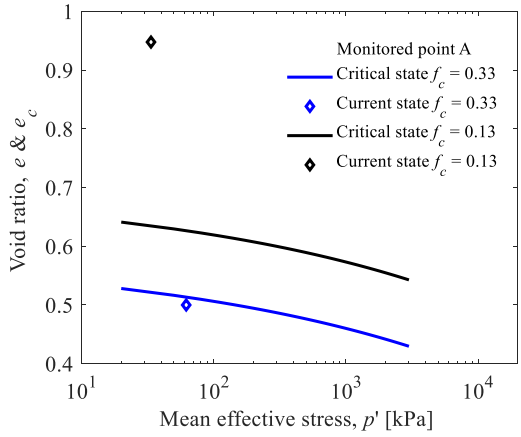

Figure 8 Movement of CSL of point A (1.2m above the top of the tunnel)

The time history of the maximum ground surface settlement is presented in Figure 9. The pore pressure reduction induced settlement (the case without erosion) in 2D conditions and the erosion induced settlement (the case with erosion) in the 2D and 3D conditions are compared.

They were normalized by the maximum ground settlement after 20 years of leakage in 2D conditions (2.2 cm). It is observed that, without the erosion process, the pore pressure reduction induced settlement developed rapidly at the beginning of the water leakage. Thereafter, it remained constant. However, for the case where the erosion of fines content was considered, the ground settlement kept increasing during 20 years of leakage. On one hand, the decrease of fines content led to the increase of the void ratio and the soil permeability increased accordingly (Eq. (8)). As a result, the pore pressure continuously decreased, leading to the consolidation of the soil. On the other hand, the CSL in the e - p' plane kept moving according to the evolution of the fines content. As a result, the strength of the eroded soil decreased, creating an unbalance between internal and external forces and, consequently, a deformation of the soil. In this case, the initial pore pressure reduction induced settlement represented only 20% of the total settlement after 20 years of leakage. Compared with the results obtained in the 2D condition, the ground settlement calculated in 3D developed far more slowly. On one hand, under the 3D condition, the constraint of the surrounding soil may limit or delay the development of the soil deformation; consequently, the plane strain and flow conditions are more conservative than the 3D condition. On the other hand, under plane strain and flow conditions, the leakage is assumed to be infinite along the longitudinal direction of the tunnel, whereas in the 3D condition, the leakage is concentrated at a point. Figure 10 shows the deviatoric plastic strain fields within the soil after 20 years of leakage for 2D and 3D models. Sliding surfaces were initiated within a loosened soil matrix due to the loss of fines. Compared with the spatial distribution of the deviatoric plastic strain in the 2D condition, the deviatoric plastic strains in the 3D condition are more localized.

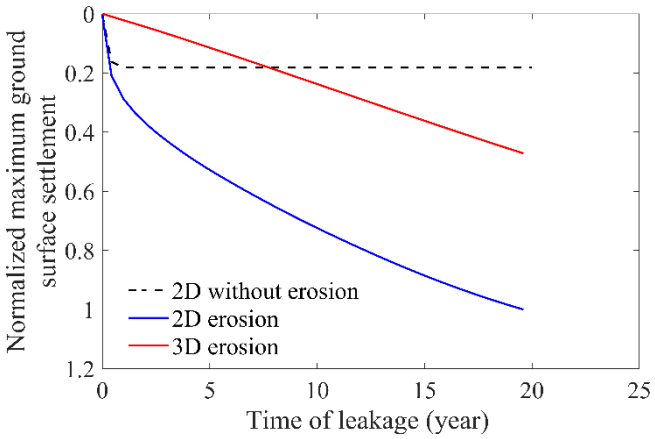

Figure 9 Time evolution of the normalized maximum ground surface settlement (normalized by the maximum ground settlement after 20 years of leakage in 2D conditions 2.2 cm)

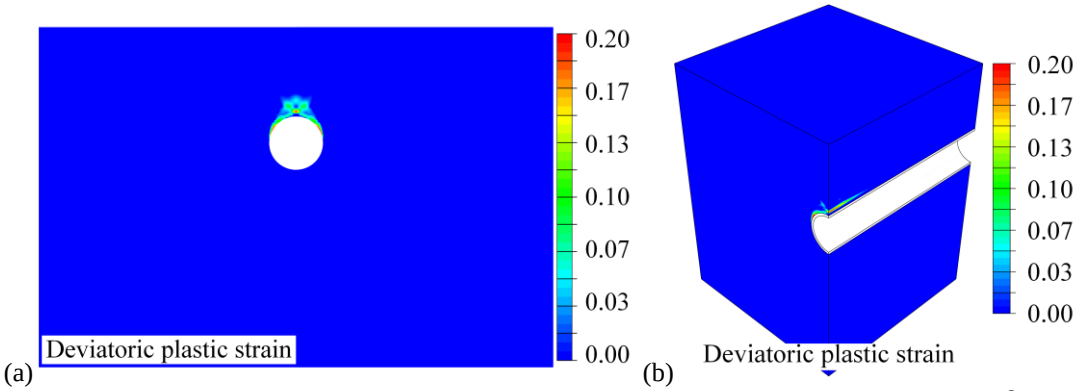

Figure 10 Spatial distribution of deviatoric plastic strain after 20 years of leakage (unit: 10^{-2}): (a) 2D model; (b) 3D model

The profiles of the calculated bending moment of the tunnel lining are presented in Figure 11. The erosion induced bending moment of the tunnel lining at the leakage point in 2D and 3D conditions were compared. They were normalized by the maximum bending moment of the tunnel lining before the leakage which is equal to 193 $kN \cdot m/m$. A significant increase in the bending moment was obtained when erosion was considered during leakage. When the erosion was not considered, the bending moment of the tunnel lining changed only slightly. The higher increase of the bending moment of the tunnel lining was obtained at the invert of the tunnel, which increased by 17% compared to the values before leakage. However, when the erosion process was considered, the loss of fines made the eroded soil around the tunnel looser and weaker, leading to the collapse of the arc effect by stress redistribution around the tunnel and, therefore, leading to the increase of the inner force in the lining. On the other hand, the void ratio increase resulted in an increase in soil permeability, leading to a decrease in the pore pressure at the eroded zone. Consequently, the inner force in the lining increased. In 2D condition, when the erosion process was considered, the bending moments increased by 65%, 72% and 50% at the top heading, the spring line, and the invert of the tunnel compared to their values before leakage. In the 3D condition, the bending moments increased by 35%, 41% and 27% at the top heading, the spring line, and the invert of the tunnel.

Overall, commonly used methods based on the pore pressure reduction (e.g. Zhang et al. [19]) cannot take into account the effect of fine soil particle loss on the permeability and mechanical properties of the eroded soil, either the strength degradation and deformation induced by soil internal erosion [57, 59, 61], thus underestimating the change in the inner force of the tunnel lining and ground movement caused by tunnel leakage. In this analysis, the pore pressure reduction induced ground settlement after 20 years of leakage accounts for only 20% of the

total settlement under plane strain and flow conditions, and the tunnel lining bending moment after pore pressure reduction does not change significantly.

Furthermore, the three-dimensional condition was shown to be a significant factor affecting the numerical results, such as the evolution of the eroded zone, the ground settlement, as well as the inner force in the tunnel lining (Figure 9 and 11). Compared with the results of plane strain calculations, the constraint of the tunnel in the out-plane direction of the soil limits the development of ground settlement under three-dimensional conditions; at the same time, under plane strain and flow conditions, the leakage is uniformly distributed along the out-plane direction of the tunnel without being able to consider the dimensions of the leakage point in that direction. Therefore, the three-dimensional condition was observed to be a significant factor affecting the process of internal erosion. In the plane strain calculation, the corresponding equivalent conversion of the water pressure or flow velocity boundary conditions at the leakage point is required.

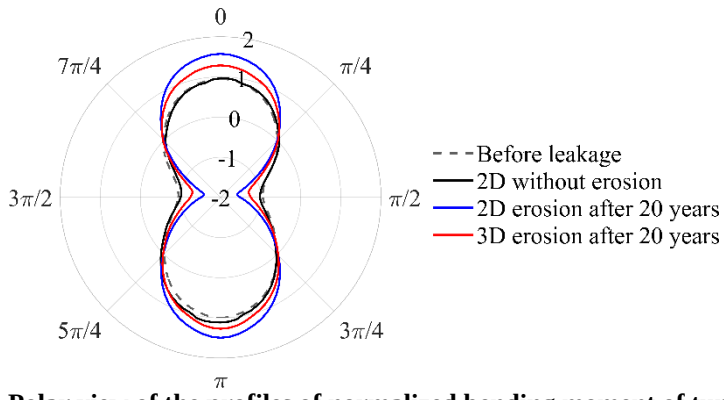

Figure 11 Polar view of the profiles of normalized bending moment of tunnel lining

5 Numerical analysis of leakage in the case of two crossing tunnels

5.1 Description of the problem

The continuous population increase and the rapid development of cities require continuously increase of land utilization, leading to a growing interest in the construction of underground space. The construction of new tunnels often needs to bypass the existing tunnels with a parallel or cross configuration. The soil disturbances induced by the newly built tunnels can result in the disturbance of the internal forces in the existing tunnel ([66]), which may lead to the great potential of tunnel leakage. The suggested numerical approach was therefore applied to study the hydro-mechanical response of two crossing tunnels constructed within a silty sand layer and experiencing a local internal erosion due to the leakage of groundwater. The influence of tunnel leakage on the tunnel-group can also be investigated in the same way.

Based on the previous numerical model (shown in Figure 3), a crossing tunnel was assumed to be located below the existing tunnel. The tunnel spacing between the tunnel central lines was set to 1.5D according to the centrifuge model test studying the effect of multi-tunnel excavations on the ground settlement [67], as shown in Figure 12, where D is the tunnel diameter. Since the study was focused on the effect of tunnel leakage, the excavation history of the crossing tunnels and the installation process of the linings were not considered. The problem was analyzed under the assumption of symmetric condition; thus, only one-quarter of the specific domain was modelled with 72943 coupled soil elements, shown in Figure 3. The groundwater level was located at the ground surface, the leakage points were assumed to be located at the top of tunnel B, as shown in Figure 12. The boundary conditions, the initial stresses, as well as the model parameters, were chosen to be the same as in the previous case.

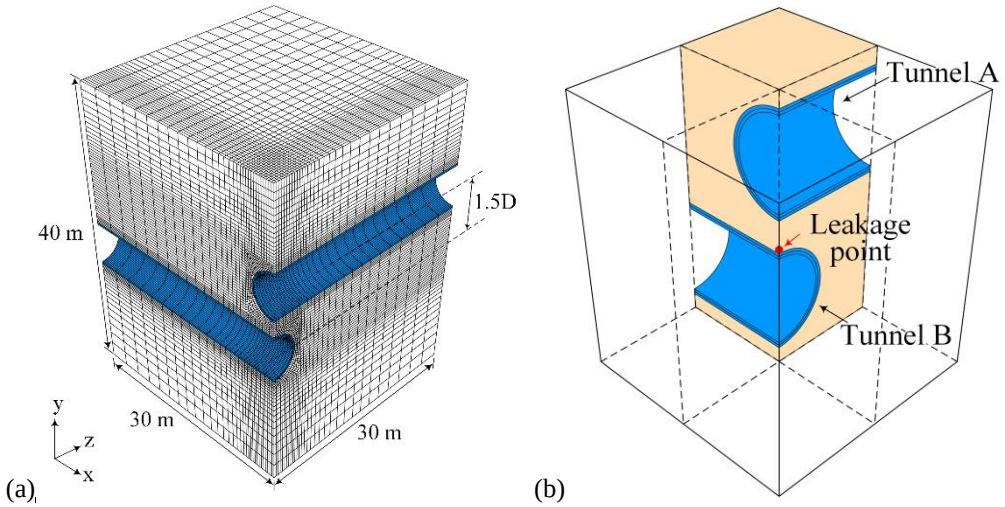

Figure 12 Numerical model for the crossing tunnels: (a) mesh of model; (b) leakage location at tunnel lining

5.2 Hydro-mechanical responses

Figure 13 shows the evolution of the fines content fields and the corresponding displacement magnitude fields during the leakage process. The eroded zone developed similarity as in the previous case. The decrease of the fines content was critical around the cavity and the eroded area developed in the direction of the maximum hydraulic gradient. Furthermore, the eroded zone developed faster around tunnel B than around tunnel A, leading to a greater ground settlement along tunnel B than along tunnel A. Figure 14 shows the deviatoric plastic strain field within the soil after 20 years of leakage. The volumetric settlements induced by a loosened soil matrix initiated the formation of a sliding surface in the vicinity of the tunnels.

Figure 15 shows the profiles of the bending moment of the tunnel lining segment at the leakage point. It can be observed that for tunnel A, when the erosion process is considered during the

leakage, the bending moments increased by 108%, 130% and 123% at the top heading, the spring line, and the invert of the tunnel compared to the values before leakage. For tunnel B, the bending moments increased by 219%, 227% and 84% at the top heading, at the spring line and the invert of the tunnel.

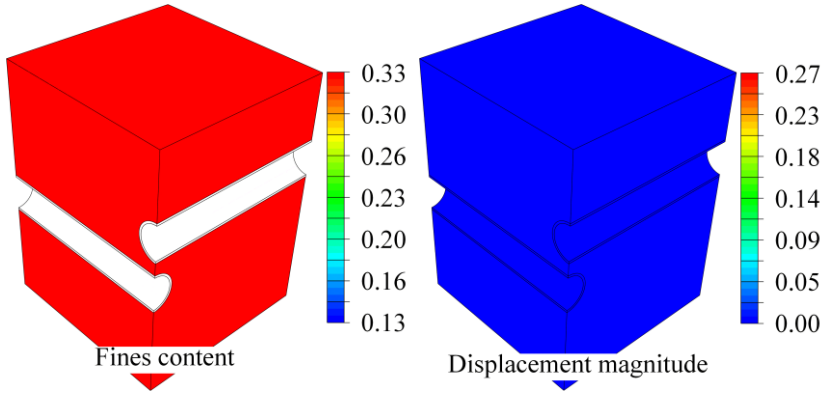

(a) Time = 0.0 years

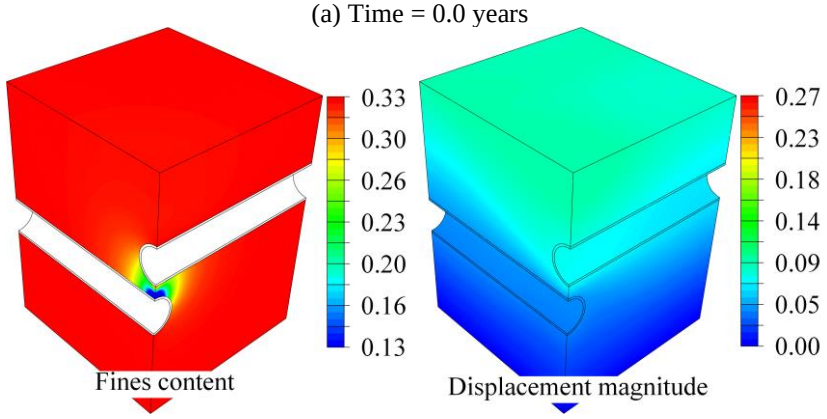

(b) Time = 7 years

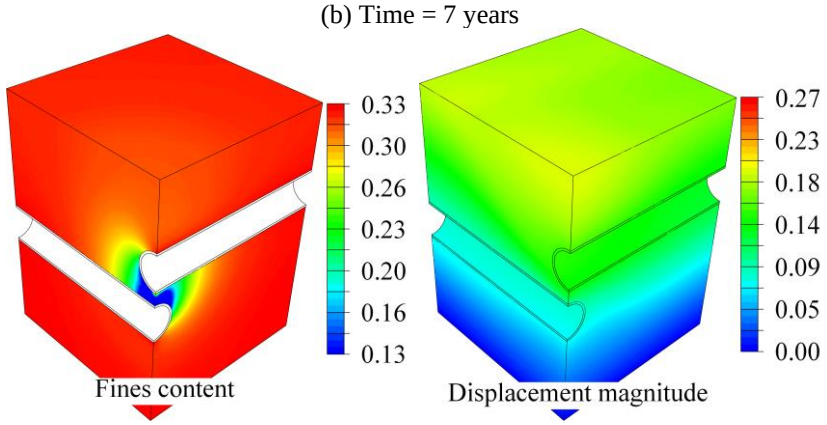

(c) Time = 14 years

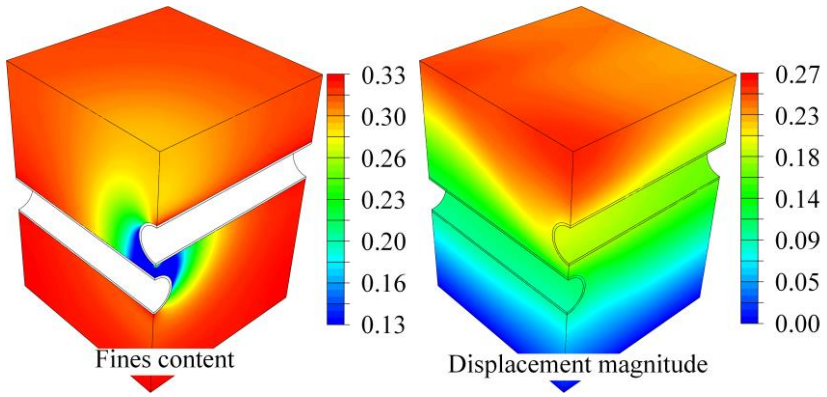

(d) Time = 20 years

Figure 13 Spatial distribution of fines content f_c and the corresponding displacement magnitude (unit: 10^{-1}m) at different times during the leakage

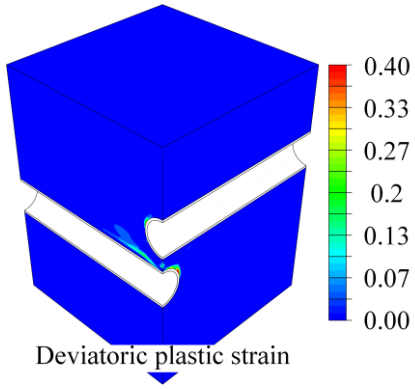

Figure 14 Spatial distribution of deviatoric plastic strain after 20 years of leakage (unit: 10^{-2})

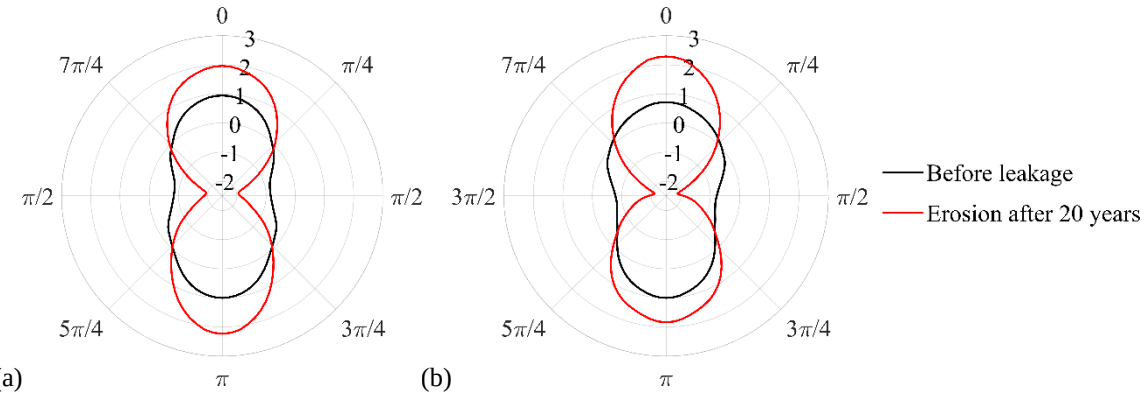

Figure 15 Polar view of the profiles of normalized bending moment of tunnel lining: (a) Tunnel A; (b) Tunnel B

It is worth pointing out that the internal erosion induced by tunnel leakage would continuously affect the redistribution of pore water pressure as well as soil strength, leading to a continuous increase of ground deformations and lining inner forces. It was observed that the internal erosion process and the induced soil deformations and inner forces in tunnel lining were highly dependent on the hydraulic boundary conditions (i.e., leakage location, leakage size, hydraulic drop, etc) and the characteristics of the tunnel (i.e., tunnel depth, multi-structure intersection, etc). The proposed numerical approach can consider reasonably well the influence of the loss of fines content induced by the leakage in the tunnel. Systematic parametric studies about the

effect of the tunnel characteristics and the hydraulic boundary conditions would surely improve the understanding of the damages induced by tunnel leakage.

6 Conclusion

In this study, the development of a coupled hydro-mechanical approach was presented, using which the effect of internal erosion induced by the local flows of tunnel leakage in saturated silty sand was investigated numerically.

The internal erosion process, i.e., the detachment and the transport of fine particles by the fluid, was modelled by the mass exchange between the solid-like and the liquid-like fine particles. The loss of fine particles due to the internal erosion affects both the void ratio and the inter-grain contact, leading to the continuous degradation of the soil strength. The mechanical behaviour of the eroded soil was described by an improved critical state-based constitutive model in which the position of the critical state line is related to the current fraction of fines content. Simultaneously, the change of the permeability induced by the evolution of the porosity leads to the further continuous reduction of the pore water pressure. This coupled model was implemented into a finite element code and then improved by using the Petrov-Galerkin weighted residual method to eliminate the spurious numerical oscillations in solving the convection dominant flow of transported particles.

The proposed approach was then applied to investigate the groundwater leakage in tunnels. The following conclusions can therefore be drawn:

(1) With the development of tunnel leakage and internal erosion, the fine particles begin to decrease at the vicinity of the leakage point resulting in a loose eroded zone. The loss of fine particles and the decrease of pore pressure lead to the soil strength degradation, the ground settlement and the additional bending moment of tunnel lining. In this analysis, for the leakage between two crossing tunnels, the bending moment of the tunnel lining could increase up to 227% compared to the values before leakage;

(2) The commonly used methods based only on pore pressure reduction cannot take into account the effect of fine soil particle loss on the permeability and mechanical properties of the eroded soil, thus underestimating the change in the inner force of the tunnel lining and ground movement caused by tunnel leakage. In this analysis, it is obtained that the pore pressure reduction induced ground settlement after 20 years of leakage accounts for only 20% of the

total settlement under plane strain and flow conditions, and the tunnel lining bending moment does not change significantly;

(3) Furthermore, the three-dimensional (3D) condition was observed to be a significant factor affecting the process of internal erosion. Compared with the results of plane strain calculations, the constraint of the tunnel in the out-plane direction of the soil limits the development of ground settlement under three-dimensional conditions; at the same time, under plane strain and flow conditions, the leakage is uniformly distributed along the out-plane direction of the tunnel without being able to consider the dimensions of the leakage point in that direction. Therefore, in the plane strain calculation, the corresponding equivalent conversion of the water pressure or flow velocity boundary conditions at the leakage point is required;

(4) Moreover, by analyzing the tunnel leakage in crossing tunnels, it is observed that the internal erosion process and the induced soil deformation and inner force in tunnel lining are highly dependent on the hydraulic boundary conditions and the tunnel characteristics. The proposed numerical approach should be a practical tool to improve the design, the construction, and to mitigate and prevent the highest risks.

It should be noted that the quantitate evolution of ground settlement and inner force of tunnel lining induced by tunnel leakage may vary if the accurate simulation of the excavation process is considered. This study is an attempt to investigate the role of internal erosion in tunnel leakage and propose a novel numerical approach to estimate the impact of water leakage into the tunnel more accurately. Even though the analyzed case was mainly theoretical, it bears a close resemblance to real case problems. These results should provide some insight for the design of future experimental and numerical investigations to understand better the physics and consequences of internal erosion in tunnel leakage. In practice, detailed case analysis can be carried out if the well-document model test or in situ data is available.

Acknowledgement

The financial supports provided by the GRF project (Grant No. 15209119) from the Research Grants Council (RGC) of Hong Kong and the National Institute for Industrial Environment and Risks of France (INERIS) are gratefully acknowledged.

Data Availability Statement

The data that support the findings of this study are available from the corresponding author upon reasonable request.

List of notations

Symbol	Description
K_0	Reference bulk modulus
υ	Poisson's ratio
n	Elastic constant controlling nonlinear stiffness
k_p	Plastic modulus
A_d	Constant controlling the magnitude of the stress-dilatancy
φ_μ	Critical friction angle
$e_{hc,cr0}$	Reference critical void ratios for pure sand
$e_{fc,cr0}$	Reference critical void ratios for pure silt
λ, ξ	Constant controlling the shape of the critical state line in the e-p' plane
a, m, f_{th}, R_d, ζ	Constant controlling the reference critical void ratio
λ_e	Constant controlling the rate of erosion rate
e_c	Critical void ratio
e_{cr0}	Reference critical void ratio
n^i	Volume fraction of constituent i
$\mathbf{v}^i$	Velocity of constituent i
$n^{ex,i}$	Volume of mass exchange among the constituents
f_c	Fraction of erodible fines
ϕ	Porosity
c	Concentration of the fluidized fines
$\mathbf{v}_s$	Velocity of the soil skeleton
$\mathbf{q}_w$	Total discharge of the pore fluid
k	Intrinsic permeability
η_k	Kinematic viscosity of the fluid
p_w	Pore fluid pressure
$\boldsymbol{g}$	Vector of the gravity field
$\bar{\rho}$	Density of the fluid mixture
ρ_s	Density of the solid
ρ_f	Density of the fluid
k_0	Initial permeability
f_{c0}	Initial fraction of erodible fines
$f_{c\infty}$	ultimate fine content fraction
α_1, α_2	Constants for the ultimate fine content fraction

$\boldsymbol{\sigma}$	Cauchy stress tensor
$\boldsymbol{\sigma}$'	Effective stress tensor
w	Unit weight
$\boldsymbol{\alpha}$	Acceleration of solid or liquid phase
$\hat{\boldsymbol{p}}$	Interaction momentum production between solid and liquid phases

Appendix: Brief introduction to the SIMSAND model

Table A1 Basic constitutive equations of SIMSAND

Components	Constitutive equations
Elasticity	$\delta\varepsilon_{ij}^{e}=\frac{1}{2G}\delta\sigma'_{ij}-\frac{\upsilon}{2G(1+\upsilon)}\delta\sigma'_{kk}\delta_{ij}$ $K=K_0\frac{(2.97-e)^2}{(1+e)}\left(\frac{p'}{p_{at}}\right)^n$
Yield surface in shear	$f_s=\frac{q}{p'}-H$
Potential surface in shear	$\frac{\partial g_s}{\partial p'}=A_d\left(M_{pt}-\frac{q}{p'}\right);\ \frac{\partial g_s}{\partial s_{ij}}=\{1\ \ 1\ \ 1\ \ 1\ \ 1\ \ 1\}$
Hardening rule for shear	$H=\frac{M_p\varepsilon_d^p}{k_p+\varepsilon_d^p}$
Critical state line and inter-locking effect	$e_c=e_{cr0}-\lambda\left(\frac{p'}{p_{at}}\right)^{\xi}$ $\tan\varphi_p=\left(\frac{e_c}{e}\right)\tan\varphi_\mu \quad \tan\varphi_{pt}=\left(\frac{e}{e_c}\right)\tan\varphi_\mu$

Table A2 Parameters of SIMSAND

Parameters	Definitions
e_0	Initial void ratio
υ	Poisson's ratio
G	Shear modulus
K_0	Reference bulk modulus
n	Elastic constant controlling nonlinear stiffness
φ_μ	Critical friction angle
e_{cr0}	Reference critical state void ratio
λ	Constant controlling the slope of CSL
ξ	Constant controlling the nonlinearity of CSL
A_d	Constant controlling the magnitude of the stress-dilatancy
k_p	Plastic modulus

References

[1] Shen S-L, Wu H-N, Cui Y-J, Yin Z-Y. Long-term settlement behaviour of metro tunnels in the soft deposits of Shanghai. Tunnelling Underground Space Technol. 2014;40( ):309-23.
[2] Jiang M, Yin Z-Y. Influence of soil conditioning on ground deformation during longitudinal tunneling. Comptes Rendus Mecanique. 2014;342(3):189-97.
[3] Jiang M, Yin Z-Y. Analysis of stress redistribution in soil and earth pressure on tunnel lining using the discrete element method. Tunnelling Underground Space Technol. 2012;32(251-9.
[4] O'reilly M, New B. Settlements above tunnels in the United Kingdom-their magnitude and prediction. The third International Symposium. England: Institution of Mining & Metallurgy, 1982. p. 173-81.
[5] Wu H-N, Shen S-L, Chai J-C, Zhang D-M, Xu Y-S. Evaluation of train-load-induced settlement in metro tunnels. Proceedings of the Institution of Civil Engineers-Geotechnical Engineering. 2014;168(5):396-406.
[6] Wu H-N, Shen S-L, Liao S-M, Yin Z-Y. Longitudinal structural modelling of shield tunnels considering shearing dislocation between segmental rings. Tunnelling Underground Space Technol. 2015;50(317-23.
[7] Li P, Du S-J, Ma X-F, Yin Z-Y, Shen S-L. Centrifuge investigation into the effect of new shield tunnelling on an existing underlying large-diameter tunnel. Tunnelling Underground Space Technol. 2014;42(59-66.
[8] Wongsaroj J, Soga K, Mair R. Tunnelling-induced consolidation settlements in London Clay. Géotechnique. 2013;63(13):1103.
[9] Zhang D, Huang Z, Yin Z, Ran L, Huang H. Predicting the grouting effect on leakage-induced tunnels and ground response in saturated soils. Tunnelling Underground Space Technol. 2017;65(76-90.
[10] Mair RJ. Tunnelling and geotechnics: new horizons. Géotechnique. 2008;58(9):695-736.
[11] El Tani M. Circular tunnel in a semi-infinite aquifer. Tunnelling Underground Space Technol. 2003;18(1):49-55.
[12] Huangfu M, Wang M-S, Tan Z-S, Wang X-Y. Analytical solutions for steady seepage into an underwater circular tunnel. Tunnelling Underground Space Technol. 2010;25(4):391-6.
[13] Park K-H, Owatsiriwong A, Lee J-G. Analytical solution for steady-state groundwater inflow into a drained circular tunnel in a semi-infinite aquifer: A revisit. Tunnelling Underground Space Technol. 2008;23(2):206-9.
[14] Zhang DM, Ma LX, Huang HW, Zhang J. Predicting leakage-induced settlement of shield tunnels in saturated clay. CMES - Computer Modeling in Engineering and Sciences. 2012;89(3):163-88.
[15] Li X. Stress and displacement fields around a deep circular tunnel with partial sealing. Comput Geotech. 1999;24(2):125-40.
[16] Li X, Flores-Berrones R. Time-dependent behavior of partially sealed circular tunnels. Comput Geotech. 2002;29(6):433-49.
[17] Shin J, Addenbrooke T, Potts D. A numerical study of the effect of groundwater movement on long-term tunnel behaviour. Geotechnique. 2002;52(6):391-403.
[18] Shin J. Analytical and combined numerical methods evaluating pore water pressure on tunnels. Géotechnique. 2010;60(2):141-5.
[19] Zhang DM, Ma LX, Zhang J, Hicher PY, Juang CH. Ground and tunnel responses induced by partial leakage in saturated clay with anisotropic permeability. Engineering Geology. 2015;189(104-15.
[20] Bonelli S, Marot D. Micromechanical modeling of internal erosion. European Journal of Environmental and Civil Engineering. 2011;15(8):1207-24.
[21] Yin Z-Y, Zhao J, Hicher P-Y. A micromechanics-based model for sand-silt mixtures. Int J Solids Struct. 2014;51(6):1350-63.

[22] Yin Z-Y, Huang H-W, Hicher P-Y. Elastoplastic modeling of sand–silt mixtures. Soils Found. 2016;56(3):520-32.
[23] Yang J, Yin Z-Y, Laouafa F, Hicher P-Y. Hydro-mechanical modeling of granular soils considering internal erosion. Can Geotech J. 2019.
[24] Yang J, Yin Z-Y, Laouafa F, Hicher P-Y. Analysis of suffusion in cohesionless soils with randomly distributed porosity and fines content. Comput Geotech. 2019;111(157-71.
[25] Yang J, Yin ZY, Laouafa F, Hicher PY. Internal erosion in dike ‐ on ‐ foundation modeled by a coupled hydromechanical approach. Int J Numer Anal Methods Geomech. 2019;43(3):663-83.
[26] Fell R, Wan CF, Cyganiewicz J, Foster M. Time for development of internal erosion and piping in embankment dams. J Geotech Geoenviron Eng. 2003;129(4):307-14.
[27] Zhang LM, Chen QUN. SEEPAGE FAILURE MECHANISM OF THE GOUHOU ROCKFILL DAM DURING RESERVOIR WATER INFILTRATION. Soils Found. 2006;46(5):557-68.
[28] Foster M, Fell R, Spannagle M. The statistics of embankment dam failures and accidents. Can Geotech J. 2000;37(5):1000-24.
[29] Yang J, Yin Z-Y, Laouafa F, Hicher P-Y. Three-dimensional hydromechanical modeling of internal erosion in dike-on-foundation. Int J Numer Anal Methods Geomech. 2020.
[30] Zhang D-M, Gao C-P, Yin Z-Y. CFD-DEM modeling of seepage erosion around shield tunnels. Tunnelling Underground Space Technol. 2019;83(60-72.
[31] Raats PAC. Applications of the theory of mixtures in soil science. Mathematical Modelling. 1987;9(12):849-56.
[32] de Boer R. Contemporary progress in porous media theory. Applied Mechanics Reviews. 2000;53(12):323-70.
[33] Borja RI. On the mechanical energy and effective stress in saturated and unsaturated porous continua. Int J Solids Struct. 2006;43(6):1764-86.
[34] Vardoulakis I, Stavropoulou M, Papanastasiou P. Hydro-mechanical aspects of the sand production problem. Transport in porous media. 1996;22(2):225-44.
[35] Yang J, Yin Z-Y, Laouafa F, Hicher P-Y. Modeling coupled erosion and filtration of fine particles in granular media. Acta Geotech. 2019;14(6):1615-27.
[36] Revil A, Cathles L. Permeability of shaly sands. Water Resources Research. 1999;35(3):651-62.
[37] Uzuoka R, Ichiyama T, Mori T, Kazama M. Hydro-mechanical analysis of internal erosion with mass exchange between solid and water. 6th International Conference on Scour and Erosion2012. p. 655-62.
[38] Cividini A, Gioda G. Finite-element approach to the erosion and transport of fine particles in granular soils. International Journal of Geomechanics. 2004;4(3):191-8.
[39] Reddi LN, Lee I-M, Bonala MV. Comparison of internal and surface erosion using flow pump tests on a sand-kaolinite mixture. Geotechnical Testing Journal. 2000;23(1):116-22.
[40] Steeb H, Diebels S, Vardoulakis I. Modeling internal erosion in porous media. Computer Applications In Geotechnical Engineering2007. p. 1-10.
[41] Cividini A, Bonomi S, Vignati GC, Gioda G. Seepage-induced erosion in granular soil and consequent settlements. International Journal of Geomechanics. 2009;9(4):187-94.
[42] Steeb H, Diebels S. A thermodynamic-consistent model describing growth and remodeling phenomena. Computational materials science. 2003;28(3):597-607.
[43] Jin YF, Yin ZY, Shen SL, Hicher PY. Selection of sand models and identification of parameters using an enhanced genetic algorithm. Int J Numer Anal Methods Geomech. 2016;40(8):1219-40.

[44] Jin Y-F, Yin Z-Y, Shen S-L, Hicher P-Y. Investigation into MOGA for identifying parameters of a critical-state-based sand model and parameters correlation by factor analysis. Acta Geotech. 2016;11(5):1131-45.
[45] Wu Z-X, Yin Z-Y, Jin Y-F, Geng X-Y. A straightforward procedure of parameters determination for sand: a bridge from critical state based constitutive modelling to finite element analysis. European Journal of Environmental and Civil Engineering. 2017:1-23.
[46] Li X-S, Wang Y. Linear representation of steady-state line for sand. J Geotech Geoenviron Eng. 1998;124(12):1215-7.
[47] Hibbitt, Karlsson, Sorensen. ABAQUS/standard User's Manual: Hibbitt, Karlsson & Sorensen, 2001.
[48] Brooks AN, Hughes TJ. Streamline upwind/Petrov-Galerkin formulations for convection dominated flows with particular emphasis on the incompressible Navier-Stokes equations. Computer methods in applied mechanics and engineering. 1982;32(1-3):199-259.
[49] Codina R. Comparison of some finite element methods for solving the diffusion-convection-reaction equation. Computer Methods in Applied Mechanics and Engineering. 1998;156(1):185-210.
[50] Donea J, Huerta A. Finite element methods for flow problems: John Wiley & Sons, 2003.
[51] Al-Khoury R. Computational modeling of shallow geothermal systems: CRC press, 2011.
[52] Zienkiewicz OC, Taylor RL. The finite element method for solid and structural mechanics: Elsevier, 2005.
[53] Yu CC, Heinrich JC. Petrov‐Galerkin methods for the time‐dependent convective transport equation. Int J Numer Methods Eng. 1986;23(5):883-901.
[54] Yu CC, Heinrich JC. Petrov—Galerkin method for multidimensional, time‐dependent, convective‐diffusion equations. Int J Numer Methods Eng. 1987;24(11):2201-15.
[55] Dammyr Ø, Nilsen B, Thuro K, Grøndal J. Possible Concepts for Waterproofing of Norwegian TBM Railway Tunnels. Rock Mechanics and Rock Engineering. 2014;47(3):985-1002.
[56] Wang F, Zhang DM, Zhu HH, Huang HW, Yin JH. Impact of overhead excavation on an existing shield tunnel: Field monitoring and a full 3D finite element analysis. Computers, Materials and Continua. 2013;34(1):63-81.
[57] Chang D, Zhang L. A stress-controlled erosion apparatus for studying internal erosion in soils. Geotechnical Testing Journal. 2011;34(6):579-89.
[58] Bendahmane F, Marot D, Alexis A. Experimental parametric study of suffusion and backward erosion. J Geotech Geoenviron Eng. 2008;134(1):57-67.
[59] Ke L, Takahashi A. Experimental investigations on suffusion characteristics and its mechanical consequences on saturated cohesionless soil. Soils Found. 2014;54(4):713-30.
[60] Yang J, Yin Z-Y, Laouafa F, Hicher P-Y. Hydromechanical modeling of granular soils considering internal erosion. Can Geotech J. 2019;57(2):157-72.
[61] Marot D, Rochim A, Nguyen H-H, Bendahmane F, Sibille L. Assessing the susceptibility of gap-graded soils to internal erosion: proposition of a new experimental methodology. Natural Hazards. 2016;83(1):365-88.
[62] Yang J, Jin Y-F, Yin Z-Y, Laouafa F, Hicher P-Y. Identifying the parameters of a hydro-mechanical model for internal erosion occurring in granular soils by using an enhanced backtracking search algorithm. European Journal of Environmental and Civil Engineering. 2020:1-20.
[63] Lee KM, Ge XW. The equivalence of a jointed shield-driven tunnel lining to a continuous ring structure. Can Geotech J. 2001;38(3):461-83.
[64] Hefny AM, Chua HC. An investigation into the behaviour of jointed tunnel lining. Tunnelling Underground Space Technol. 2006;21(3-4):428.

[65] Teachavorasinskun S, Chub-uppakarn T. Influence of segmental joints on tunnel lining. Tunnelling Underground Space Technol. 2010;25(4):490-4.
[66] Jin Y-F, Zhu B-Q, Yin Z-Y, Zhang D-M. Three-dimensional numerical analysis of the interaction of two crossing tunnels in soft clay. Underground Space. 2019;4(4):310-27.
[67] Divall S, Goodey RJ. Twin-tunnelling-induced ground movements in clay. Proceedings of the Institution of Civil Engineers - Geotechnical Engineering. 2015;168(3):247-56.

Figure captions

Figure 1 Scheme of the shield tunnel in the numerical analysis

Figure 2 Illustration of leakage points in the shield precast tunnel: (a) re-annotated after Dammyr et al. [55]; (b) Leakage of the shield tunnel in saturated soils in Shanghai

Figure 3 Mesh of the numerical models: (a) 2D model (1/2 model due to symmetry); (b) 3D model (1/4 model due to symmetry)

Figure 4 leakage location at tunnel lining: (a) 2D model; (b) 3D model

Figure 5 Spatial distribution of fines content *fc* and the corresponding displacement magnitude (unit: 10-1m) in 2D condition at different times during the leakage

Figure 6 Spatial distribution of fines content *fc* and the corresponding displacement magnitude (unit: 10-1m) in 3D condition at different times during the leakage

Figure 7 Profiles of pore pressure distribution above the tunnel: (a) without erosion; (b) with erosion

Figure 8 Movement of CSL of point A (1.2m above the top of the tunnel)

Figure 9 Time evolution of the normalized maximum ground surface settlement

Figure 10 Spatial distribution of deviatoric plastic strain after 20 years of leakage (unit: 10-2): (a) 2D model; (b) 3D model

Figure 11 Polar view of the profiles of normalized bending moment of tunnel lining

Figure 12 Numerical model for the crossing tunnels: (a) mesh of model; (b) leakage location at tunnel lining

Figure 13 Spatial distribution of fines content *fc* and the corresponding displacement magnitude (unit: 10-1m) at different times during the leakage

Figure 14 Spatial distribution of deviatoric plastic strain after 20 years of leakage (unit: 10-2)

Figure 15 Polar view of the profiles of normalized bending moment of tunnel lining: (a) Tunnel A; (b) Tunnel B